Check for updates

T_m filtering by ^{1}H-methyl labeling in a deuterated protein for pulsed double electron–electron resonance EPR†

Thomas Schmidt and G. Marius Clore 🄳 *

Modulating the phase-memory relaxation time (T_m) of a spin label by introducing ^{1}H-methyl groups in a perdeuterated protein background is used in DEER experiments to assign interactions in multimodal $P(r)$ distributions. Proof of principle is demonstrated using Protein A where one nitroxide label occupies two distinct regions of conformational space. The presence of a single protonated methyl group in close proximity (4–8 Å) to only one of the two nitroxide rotamer ensembles results in a selective and substantial decrease in T_m, manifested by differential decay of the peak intensities in the bimodal $P(r)$ distance distribution as a function of the total dipolar evolution time. This form of T_m filtering will facilitate DEER structural analysis of biomolecular systems with three spin labels, including complexes involving multimeric proteins.

Pulsed double electron–electron resonance (DEER) EPR spectroscopy provides a means of accurately measuring long-range distances between pairs of spin labels and, as such, is an invaluable tool for conformational analysis of proteins and other biological macromolecules.[1,2] With complete deuteration of both protein and solvent, distances up to 170 Å can potentially be measured.[3–5] When more than two spin labels are present, analysis can prove challenging, not only due to artefacts arising from multi-spin effects[1,6,7] but because assignment of distances to specific interactions between paramagnetic centres may be difficult a priori. One approach to resolve this issue makes use of orthogonal spin-labeling to probe interactions between different spin labels (*e.g.*, a nitroxide and a paramagnetic metal centre such as Gd^{3+} or Cu^{2+}) separately from those between like spin labels.[8–11] Here we propose another strategy that makes use of specific ^{1}H methyl labeling in a perdeuterated protein background,[12] thereby permitting phase-memory relaxation time (T_m) filtering in DEER, analogous to T_2 filtering in solution

Laboratory of Chemical Physics, National Institute of Diabetes and Digestive and Kidney Diseases, National Institutes of Health, Bethesda, Maryland 20892-0520, USA. E-mail: mariusc@mail.nih.gov

NMR.[13] We demonstrate this approach on a model system, Protein A, in which one of the nitroxide spin labels occupies two distinct regions of conformational space giving rise to two separate distances in the DEER-derived $P(r)$ probability distance distribution.

The model system employed is AviTag-Protein A with the nitroxide spin label (R1) attached to engineered cysteine residues close to the N- (Q39C) and C- (K88C) termini of the ordered Protein A domain (residue numbering according to the complete construct which includes the AviTag; the Protein A domain extends from residues 30 to 90, and residues 1–38 are disordered).[14] Previous Q-band DEER has shown the presence of two clearly resolved distances in the $P(r)$ distribution, at 33 and 38 Å,[14] arising from the Q39C-R1 label occupying two distinct regions of conformational space (labeled *a* and *b* in Fig. 1A), as judged by the predicted $P(r)$ distribution generated from the atomic coordinates using the spin-label rotamer library program MMM.[15,16]

Hahn spin echo decay curves recorded with a two-pulse Hahn echo sequence (ESI,† Fig. S1A) with the nitroxide label either at the N- (Q39C-R1; Fig. 1A) or C (K88C-R1; Fig. 1B) terminal ends of the ordered Protein A domain were recorded on four samples of AviTag-Protein A in fully deuterated solvent (70% D_2O/30% d_8-glyerol v/v): fully deuterated, fully protonated, and either Leu ($C^{\delta 1}H_3$ and $C^{\delta 2}H_3$) or Ile ($C^\delta H_3$) methyl-protonated on a perdeuterated background (see ESI† for details of protein expression, purification, nitroxide labeling, deuteration, and incorporation of protonated Leu or Ile methyl groups). There are 7 leucines (Fig. 1A, right) and 2 isoleucines (Fig. 1B, right). The apparent T_m (T_m^{app}) values for the fully deuterated and fully protonated samples are ∼35 and 9 µs, respectively (Fig. 1A and B). For Q39C-R1, the introduction of Leu ^{1}H-methyl groups in a perdeuterated background results in a two-fold reduction in the T_m^{app} value to ∼17 µs (Fig. 1A); no reduction in T_m^{app}, however, is observed for the corresponding K88C-R1 sample (Fig. 1B). Introduction of $C^\delta H_3$ methyl-protonated Ile in a perdeuterated background results in only a minimal reduction in the T_m^{app} value (to ∼32 µs) for both the
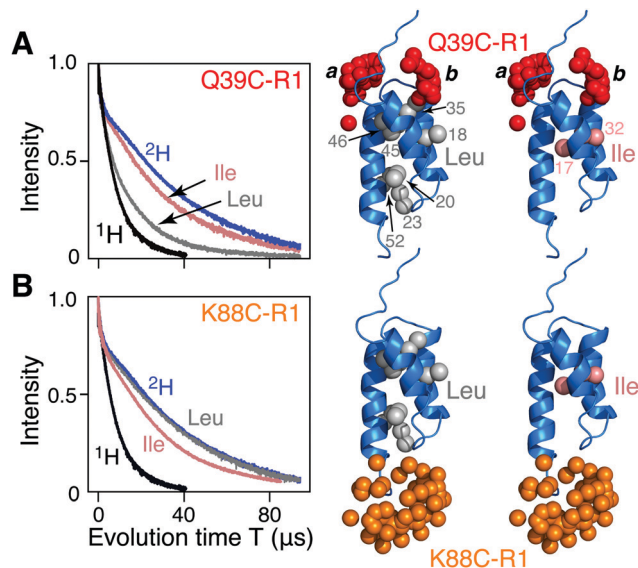
Fig. 1 Two-pulse Hahn spin-echo decay curves for nitroxide spin-labeled AviTag-Protein A. The left hand panels show the spin echo curves for fully deuterated (blue), fully protonated (black), and Leu (grey) and Ile (pink) methyl protonated in a deuterated background samples of AviTag-Protein A nitroxide spin labeled at either (A) Q39C-R1 or (B) K88C-R1. The pulse scheme used is shown in Fig. S1A (ESI†). The left hand panels show the corresponding backbone ribbon diagram of Protein A (blue; PDB code 1BDD)[22] with the methyl groups of Leu or Ile ($C^\delta H_3$) shown as grey and pink spheres, respectively, and the oxygen atoms of the calculated Q39C-R1 and K88C-R1 ensembles in red and orange, respectively. The nitroxide label ensembles were calculated from the atomic coordinates using the nitroxide rotamer library program MMM. The Q39C-R1 spin label samples two distinct regions of conformational spaces indicated by the labels a and b; only b is close to a methyl group.

Q39C-R1 and K88C-R1 samples (Fig. 1A and B), and it seems likely that this small reduction may in fact be due to the presence of a small amount of residual H_2O owing to incomplete exchange with the D_2O buffer. It has previously been shown that protons, and especially methyl groups in close proximity (4–8 Å) to the unpaired electron of a nitroxide spin label are the largest contributor to transverse electron relaxation,[17–21] and examination of the Protein A structure (Fig. 1, right panels) shows that our results are fully consistent with this phenomenon, since only the Q39C-R1 spin label in conformer b is sufficiently close to a methyl group (specifically the two methyls of Leu35; Fig. 1A and also Fig. S2, ESI†) to induce a significant reduction in T_m^{app}.

Fig. 2 presents the results for Leu methyl-protonated, otherwise deuterated [Leu-CH_3/^2H]-AviTag-Protein A spin-labeled at both Q39C-R1 and K88C-R1 (Fig. 2A). As expected, the T_m^{app} for the Hahn spin-echo decay curve of the Q39C-R1/K88C-R1 doubly-spin labeled sample is intermediate between that for the Q39C-R1 and K88C-R1 single spin-labeled samples (Fig. 1B). DEER data were recorded with a refocussed four-pulse scheme (Fig. S1B, ESI†)[23] varying the length of the second echo period T (= $2\tau_2$), keeping the length of the acquisition time t_{max} constant at 4 μs, with the exception of the data at τ_2 = 4 μs, where t_{max} was set to 3 μs (Fig. S3 and ESI† Methods). For t_{max} = 3 and 4 μs, the upper limits for an accurate mean
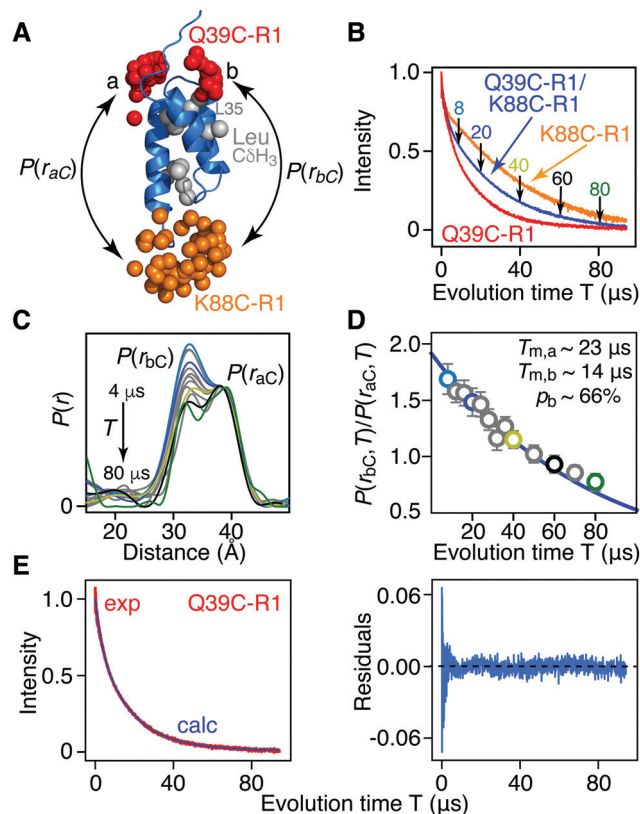

Fig. 2 Phase memory relation time (T_m) filtering for [Leu-CH_3/^2H] AviTag-Protein A (Q39C-R1/K88C-R1) in an otherwise perdeuterated background. (A) Ribbon diagram of the protein A core domain[22] (blue) with the oxygen atoms of the nitroxide spin label ensembles (generated using the rotamer library program MMM) colored in red (Q39C-R1) and orange (K88C-R1), and the leucine methyl groups in grey. The two distances between K88C-(R1) and the two conformer populations (a and b) of Q39C-R1 are indicated. (B) Hahn spin-echo curves for [Leu-CH_3/^2H] AviTag-Protein A, spin-labeled at Q39C-R1/K88C-r1 (blue), Q39C-R1 (red) and K88C-R1 (orange). (C) $P(r)$ distributions for [Leu-CH_3/^2H] AviTag-Protein A (Q39C-R1/K88C-R1) obtained from the DEER echo curves using DeerAnalysis[24] with Tikhonov regularization at evolution times T (= $2\tau_2$) ranging from 8 to 80 μs. The color coding corresponds to that of the experimental points in panel D. The $P(r)$ distributions are normalized with regard to the a peak at 38 Å. The DEER pulse scheme is shown in Fig. S1B (ESI†), and the raw and background-corrected DEER echo curves are shown in Fig. S3 (ESI†). Results of global best-fitting eqn (1) and (2) to the experimental evolution time T (= $2\tau_2$) dependence of (D) the peak intensity ratio,$P(r_{bC},T)/P(r_{aC},T)$, in the $P(r)$ distributions for [Leu-CH_3/^2H] AviTag-Protein A (Q39C-R1/K88C-R1) and (E) the Hahn echo curve for [Leu-CH_3/^2H] AviTag-Protein A (Q39C-R1) (left panel). The experimental ratios of the b to a peak intensities, $P(r_{bC},T)/P(r_{aC},T)$, are obtained from the integrated intensities of two Gaussians fitted to the bimodal $P(r)$ distributions. The experimental data and best-fits are displayed by the circles and blue line, respectively in (D) and by the red and blue curves, respectively, in (E). Normalization in (E) was carried out by dividing the experimental and calculated curves by the optimized value of the sum of the two scale factors ($\lambda_1 + \lambda_2$). The right panel in (E) is a plot of the distribution of residuals between experimental and calculated Hahn echo curves. The corresponding $P(r)$ distributions and best fits obtained using DeerAnalysis with validated Tikhonov regularization,[24] the program DD with a sum of two Gaussians,[25] the program WavPDS (to filter out noise)[26] followed by Tikhonov regularization,[24] and WavPDS followed by SVD[26–28] are shown in Fig. S4–S7 (ESI†), respectively.

distance determination are $50(t_{max}/2)^{1/3}$ = 57 and 63 Å, respectively; the upper limits for an accurate determination of the

width of the $P(r)$ distribution are $40(t_{max}/2)^{1/3}$ = 46 and 50 Å, respectively.[1] The DEER echo curves were analysed to generate $P(r)$ distributions using five different methods: model free Tikhonov regularization with the program DeerAnalysis without (Fig. 2C) and with (Fig. S4A, ESI†) validation;[24] the program DD in which the DEER data are modelled as originating from the sum of two Gaussians (Fig. S5A, ESI†);[25] the program WavPDS (wavelets for pulse dipolar signals) to filter out noise using a wavelet denoising method,[26] followed by Tikhonov regularization[24] (Fig. S6A, ESI†); and WavPDS followed by singular value decomposition (SVD) (Fig. S7A, ESI†).[27,28] Since model-independent Tikhonov regularization, model-dependent Gaussian modelling and model-independent SVD represent three completely different approaches for extracting $P(r)$ distributions from DEER echo curves, a comparison of the results provides an independent means of assessing the accuracy of the resulting $P(r)$ distributions.[29,30] All five methods of analysis yield quantitatively very similar results, in which the integrated intensity of the b component of the bimodal $P(r)$ distribution centred at $\sim$33 Å decays more rapidly than that of the a component centred at $\sim$38 Å. Thus, one can immediately conclude that the T_m of the b component is shorter than that of the a component as a consequence of increased transverse electron relaxation arising from close proximity of the ^{1}H-methyl groups of Leu35 to the unpaired electron in the b ensemble of the Q39C-R1 spin label (Fig. 2A).

The ratio of the integrated intensity of the b to a components of the $P(r)$ distribution, $P(r_{bC},T)/P(r_{aC},T)$, for [Leu-CH$_3$/^{2}H]-AviTag-Protein A (Q39C-R1/K88C-R1) shown in Fig. 2D, is expected to decay as:

$$P(r_{bC},T)/P(r_{aC},T) = p_b/(1 - p_b)\exp[-T(R_m^b - R_m^a)/2] \qquad (1)$$

where p_b is the occupancy of the Q39C-R1 nitroxide in the b state, and R_m^b (= $1/T_m^b$) and R_m^a (= $1/T_m^a$) are the phase-memory relaxation rates for Q39C-R1 in the b and a states, respectively. (Note that when taking the ratio of the integrated intensities of the two peaks in the $P(r)$ distribution, the contribution to phase-memory relaxation from the second spin label at K88C-R1 is cancelled out). The signal intensity, $S(T)$ of the Hahn spin echo curve for [Leu-CH$_3$/^{2}H]-AviTag-Protein A (Q39C-R1) (Fig. 2E) is given by the sum of three exponentials:

$$S(T) = \lambda_1 \exp(-R_{ESEEM}T) + \lambda_2[(1 - p_b)\exp(-TR_m^a) + p_b \exp(-TR_m^b)] \qquad (2)$$

where λ_1 and λ_2 are scale factors and R_{ESEEM} is the apparent relaxation rate to account for the very fast initial decay of the spin echo curve due to electron spin echo envelope modulation (ESEEM). Simultaneous fitting of the data in Fig. 2D and E using eqn (1) and (2), yields values of $\sim$23 and 14 μs for T_m^a and T_m^b, respectively with a b state occupancy of $\sim$66%. The optimized values of the relaxation rates and occupancy of the b state are quantitatively the same (within experimental error) for the $P(r)$ distributions obtained using all five methods of processing the DEER data to generate the $P(r)$ distributions, and are summarized in Table 1.

Table 1 Optimized values of the phase memory relaxation rates (R_m) for the a and b populations of the Q39C-R1 spin label in [Leu-CH$_3$/^{2}H]-AviTag-Protein A, the occupancy of the b state (p_B), and the apparent relaxation rate, R_{ESEEM}, for the initial fast decay of the Hahn spin echo curve due to the ESEEM effect

Method[ab]	R_m^a (ms^{-1})	R_m^b (ms^{-1})	p_B	R_{ESEEM} (ms^{-1})
DA[c]	44.3 ± 0.4	70.1 ± 0.5	0.66 ± 0.01	352 ± 7
DA with validation[d]	47.5 ± 0.4	67.2 ± 0.5	0.63 ± 0.01	321 ± 7
DD	46.8 ± 0.7	67.0 ± 0.7	0.66 ± 0.01	326 ± 9
WavPDS + DA	45.8 ± 0.4	69.3 ± 0.4	0.64 ± 0.01	322 ± 7
WavPDS + SVD	46.9 ± 0.4	69.3 ± 0.4	0.60 ± 0.01	329 ± 8

[a] Method used to derive the $P(r)$ distributions from the DEER echo curves. The values of the two scale factors, λ_1 and λ_2, describing the amplitudes of the contributions of the ESEEM effect and phase-memory relaxation, respectively, to the Hahn spin echo curves are given in Table S1 (ESI). [b] The reduced χ^2 of the global fits are as follows: DA (DeerAnalysis), 1.09; DA with validation, 1.09; DD, 1.10; WavPDS + DA, 1.10; WavPDS + SVD, 1.13. [c] DA with Tikhonov regularization. [d] Validated Tikhonov regularization was carried out varying the modulation depth (11 steps from 0.25 to 0.5), background density (11 steps from 0.04 to 0.15) and background start (6 steps from 500 to 1800 ns) for a total of 726 permutations.

For [Ile-C$^\delta$H$_3$/^{2}H] AviTag-Protein A (Fig. 3A), on the other hand, no difference in apparent T_m is observed between singly spin labeled (Q39C-R1 or K88C-R1) or doubly spin labeled (Q39C-R1/K88C-R1) samples (Fig. 3B), and no change in the ratio of peak intensities of the a and b components is observed in the DEER derived $P(r)$ distributions obtained with evolution times T (= $2\tau_2$) ranging from 10 to 60 μs (Fig. 3C and D). This is as expected, as the two Ile C$^\delta$H$_3$ methyl groups are not in close proximity to either the Q39C-R1 or K88C-R1 spin label (Fig. 3A and Fig. S2, ESI†), and provides a control for the results obtained with the [Leu-CH$_3$/^{2}H] labeling.

In summary, we have shown that the introduction of a protonated methyl group(s) in an otherwise fully deuterated background, located in close proximity (less than 8 Å) to a nitroxide spin label can be used as a T_m filter in DEER spectroscopy. The example presented here of AviTag-Protein A provides proof of principle as the presence of a bimodal $P(r)$ distribution is due to two distinctly different regions of conformational space sampled by one of the spin labels (specifically Q39C-R1). However, one can readily envision applications involving complexes between multimeric proteins. For example, in a complex between monomeric and homodimeric proteins the presence of three spin labels cannot be avoided if one wishes to probe distances between the two partner proteins in the complex. When the methyl group(s) is close to the nitroxide spin label in each subunit of the dimer, the relative contribution of the intersubunit distance can be selectively reduced by T_m filtering in the DEER-derived $P(r)$ distribution relative to those of the intermolecular distances between monomer and dimer; conversely, a methyl group close to the nitroxide spin label on the monomer can be used to selectively reduce the contribution of the distances between monomer and dimer relative to the intersubunit distance within the dimer. Similar applications can be envisaged in the context of assigning interactions in monomeric proteins spin-labeled at three sites simultaneously.
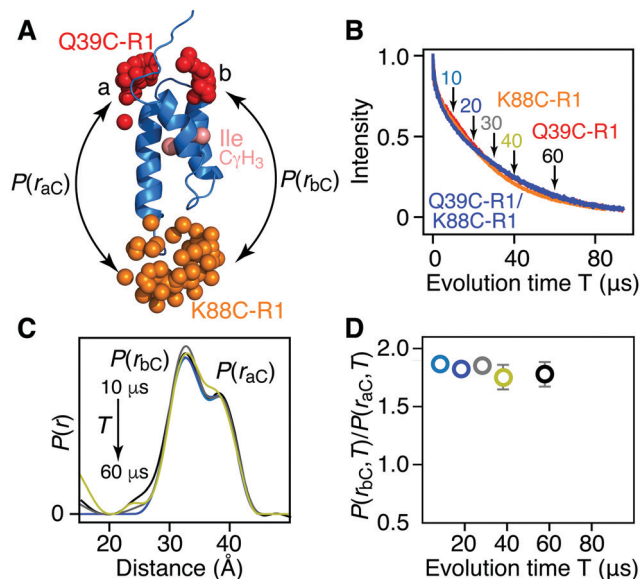
Fig. 3 Introduction of protonated Ile $C^{\delta}H3$ methyl groups in a deuterated background has no effect on T_m or DEER-derived $P(r)$ distributions for AviTag-Protein A spin labeled at Q39C-R1 and/or K88C-R1. (A) Ribbon diagram of the protein A core domain (blue), with the oxygen atoms of the nitroxide spin label ensembles (generated using the rotamer library program MMM) colored in red (Q39C-R1) and orange (K88C-R1), and the Ile $C^{\delta}H_3$ methyl groups in pink. The two distances between K88C-(R1) and the two conformer populations (a and b) of Q39C-R1 are indicated. (B) Hahn spin-echo curves for [Ile-$C^{\gamma}H3/^2H$] AviTag-Protein A, spin-labeled at Q39C-R1/K88C-r1 (blue), Q39C-R1 (red) and K88C-R1 (orange). (C) $P(r)$ distributions for [Ile-$C^{\gamma}H3/^2H$] AviTag-Protein A (Q39C-R1/K88C-R1) obtained from the DEER echo curves using DeerAnalysis[24] with Tikhonov regularization at evolution times T (= $2\tau_2$) ranging from 10 to 60 μs. The color coding corresponds to that of the experimental points in panel D. The $P(r)$ distributions are normalized with regard to the a peak at 38 Å. The raw and background-corrected DEER echo curves are shown in Fig. S8 (ESI†). (D) Dependence of the peak intensity ratio, $P(r_{bC},T)/P(r_{aC},T)$, in the $P(r)$ distributions for [Ile-$C^{\gamma}H3/^2H$] AviTag-Protein A (Q39C-R1/K88C-R1) on evolution time T (= $2\tau_2$). The ratios of b to a peak intensities, $P(r_{bC},T)/P(r_{aC},T)$, are obtained from the integrated intensities of two Gaussians fitted to the bimodal $P(r)$ distributions. The same results are obtained when the DEER echo curves are processed using the programs DeerAnalysis with validated Tikhonov regularization (Fig. S9, ESI†),[24] DD with two Gaussians,[25] WavPDS[26] followed by Tikhonov regularization,[24] and WavPDS followed by SVD[26,28] (Fig. S10, ESI†).

Conflicts of interest

There are no conflicts to declare.

Notes and references

1 G. Jeschke, Annu. Rev. Phys. Chem., 2012, 63, 419–446.
2 O. Duss, M. Yulikov, F. H. T. Allain and G. Jeschke, Methods Enzymol., 2015, 558, 279–331.
3 R. Ward, A. Bowman, E. Sozudogru, H. El-Mkami, T. Owen-Hughes and D. G. Norman, J. Magn. Reson., 2010, 207, 164–167.
4 H. El Mkami and D. G. Norman, Methods Enzymol., 2015, 564, 125–152.
5 T. Schmidt, M. A. Walti, J. L. Baber, E. J. Hustedt and G. M. Clore, Angew. Chem., Int. Ed., 2016, 55, 15905–15909.
6 G. Jeschke, M. Sajid, M. Schulte and A. Godt, Phys. Chem. Chem. Phys., 2009, 11, 6580–6591.
7 T. von Hagens, Y. Polyhach, M. Sajid, A. Godt and G. Jeschke, Phys. Chem. Chem. Phys., 2013, 15, 5854–5866.
8 E. Narr, A. Godt and G. Jeschke, Angew. Chem., Int. Ed., 2002, 41, 3907–3910.
9 P. Lueders, G. Jeschke and M. Yulikov, J. Phys. Chem. Lett., 2011, 2, 604–609.
10 A. Meyer, D. Abdullin, G. Schnakenburg and O. Schiemann, Phys. Chem. Chem. Phys., 2016, 18, 9262–9271.
11 A. Meyer and O. Schiemann, J. Phys. Chem. A, 2016, 120, 3463–3472.
12 V. Tugarinov, V. Kanelis and L. E. Kay, Nat. Protoc., 2006, 1, 749–754.
13 F. Rastrelli, S. Jha and F. Mancin, J. Am. Chem. Soc., 2009, 131, 14222–14224.
14 J. L. Baber, J. M. Louis and G. M. Clore, Angew. Chem., Int. Ed., 2015, 54, 5336–5339.
15 Y. Polyhach, E. Bordignon and G. Jeschke, Phys. Chem. Chem. Phys., 2011, 13, 2356–2366.
16 G. Jeschke, Protein Sci., 2018, 27, 76–85.
17 M. Lindgren, G. R. Eaton, S. S. Eaton, B. H. Jonson, P. Hammarström, M. Svensson and J. Carlsson, J. Chem. Soc., Perkin Trans. 2, 1997, 2549–2554.
18 M. Persson, J. R. Harbridge, P. Hammarstrom, R. Mitri, L. G. Martensson, U. Carlsson, G. R. Eaton and S. S. Eaton, Biophys. J., 2001, 80, 2886–2897.
19 M. Huber, M. Lindgren, P. Hammarstrom, L. G. Martensson, U. Carlsson, G. R. Eaton and S. S. Eaton, Biophys. Chem., 2001, 94, 245–256.
20 H. El Mkami, R. Ward, A. Bowman, T. Owen-Hughes and D. G. Norman, J. Magn. Reson., 2014, 248, 36–41.
21 E. R. Canarie, S. M. Jahn and S. Stoll, J. Phys. Chem. Lett., 2020, 11, 3396–3400.
22 H. Gouda, H. Torigoe, A. Saito, M. Sato, Y. Arata and I. Shimada, Biochemistry, 1992, 31, 9665–9672.
23 M. Pannier, S. Veit, A. Godt, G. Jeschke and H. W. Spiess, J. Magn. Reson., 2000, 142, 331–340.
24 G. Jeschke, V. Chechik, P. Ionita, A. Godt, H. Zimmerman, J. E. Banham, C. R. Timmel, D. Hilger and H. Jung, Appl. Magn. Reson., 2006, 30, 473–498.
25 S. Brandon, A. H. Beth and E. J. Hustedt, J. Magn. Reson., 2012, 218, 93–104.
26 M. Srivastava, E. R. Georgieva and J. H. Freed, J. Phys. Chem. A, 2017, 121, 2452–2465.
27 M. Srivastava and J. H. Freed, J. Phys. Chem. Lett., 2017, 8, 5648–5655.
28 M. Srivastava and J. H. Freed, J. Phys. Chem. A, 2019, 123, 359–370.
29 T. Schmidt, J. Jeon, Y. Okuno, S. C. Chiliveri and G. M. Clore, ChemPhysChem, 2020, 21, 1224–1229.
30 T. Schmidt, J. M. Louis and G. M. Clore, ChemBioChem, 2020, DOI: 10.1002/cbic.202000263.